BL11XU
QST Quantum Dynamics I

1. Introduction

BL11XU is an in-vacuum undulator beamline operated by the National Institutes for Quantum Science and Technology (QST). It is designed to provide scientists and engineers with a wide range of options on advanced synchrotron radiation and quantum functional material research. In BL11XU, switchable Si(111) and Si(311) double-crystal monochromators cooled by liquid nitrogen are installed in the optical hutch. Highly brilliant and well-collimated synchrotron X-rays are available in the energy range of 6–70 keV. There are three experimental hutches; each one contains specialized measurement instruments for studies using Mössbauer spectroscopy (EH1), inelastic X-ray scattering and X-ray magnetic circularly polarized emission (EH2), and surface X-ray diffraction (EH3).

2. Mössbauer spectroscopy

Negative spin polarization materials generate a spin current whose spin direction is opposite to the magnetization direction. This nature is important because it increases the freedom in the design of spintronic devices. Recently, we have studied FeCr from the viewpoints of band structure to explore its potentiality as a negative spin polarization material. The calculations on the disordered FeCr alloy predicted a high negative spin polarization, which is attributed to the band matching of the minority spin. In addition, we experimentally fabricated $Fe_{1-x}Cr_x$ films in the Cr concentration (x) range from 0.2 to 0.4 by sputter deposition and demonstrated inverse magnetoresistance using current perpendicular to plane giant magnetoresistance (GMR) devices, which provided evidence of negative spin polarization. However, the spin polarization of $Fe_{0.7}Cr_{0.3}$ estimated from the GMR device measurements was –0.28 and fell below the calculated value.

To explore the origin of the discrepancy between experiment and theory, the microstructure of FeCr alloys was studied using synchrotron Mössbauer spectroscopy [1]. The experiments were conducted at BL11XU of SPring-8. The π-polarized Mössbauer γ-rays were incident on each nonenriched sample surface at an angle of 0.14°. The γ-ray penetration depth was a few nanometers. A magnetic field of 90 mT was applied along the sample plane and parallel to the magnetic unit vector of the π-polarized Mössbauer γ-rays. In this configuration, the incident γ-rays interacted with the two nuclear transitions with $\Delta m = 0$.

Figure 1(a) shows the Mössbauer spectrum of the as-deposited $Fe_{0.7}Cr_{0.3}$ (20 nm) film. Two absorption dips originating from the two nuclear transitions with $\Delta m = 0$ were observed. The broad width of the dips is attributed to the hyperfine magnetic field (H_{hf}) distribution due to variations in the Cr atom arrangement around the Fe atoms. The calculated H_{hf} distribution shown in Fig. 1(b) is broad and can be decomposed into four Gaussian components having centers at 11.4, 18.1, 22.6, and 28.3 T. The result indicates that inhomogeneity exists in the as-deposited state, owing to the phase separation nature of the Fe-Cr system. The average H_{hf} and isomer shift (IS) values are shown in Table 1.

Figures 1(c) and 1(e) show the Mössbauer spectra obtained after annealing at 220 and 400°C for 5 h, respectively. Figures 1(d) and 1(f) show the corresponding H_{hf} distribution. For ease of comparison, data for the as-deposited sample are also shown. After annealing at 220°C, the H_{hf} distribution increased above 31 T and decreased below 31 T. Considering that H_{hf} of pure Fe is 33 T, this change can be attributed to the development of Fe-rich regions or clustering of Fe atoms. This trend evolved further after annealing at 400°C, and there was an overall shift toward the higher field side. The average H_{hf} and *IS* shown in Table 1 both increased as the annealing temperature increased, which supports the development of Fe-rich regions.

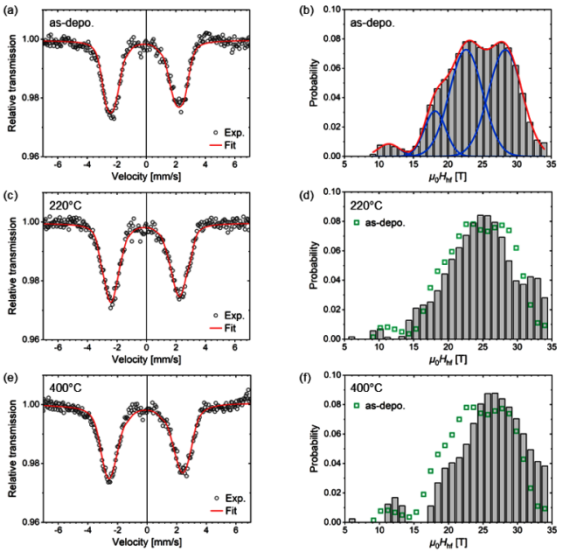

Fig. 1. (a), (c), and (e) Mössbauer spectra of $Fe_{0.7}Cr_{0.3}$(20nm) thin film for different annealing conditions. (b), (d), and (f) H_{hf} distribution. Fitting by four Gaussian functions is depicted in (b), and the data in (b) are also plotted in (d) and (f) for ease of comparison.

Table 1. Mössbauer parameters derived from the data analysis.

	Average $\mu_0 H_{hf}$ [T]	Average IS [mm/s]
As-depo.	24.2	−0.11
220°C	24.7	−0.097
400°C	25.8	−0.09

In summary, synchrotron Mössbauer experiments indicated that the as-deposited FeCr composition was inhomogeneous and that Fe-rich regions formed after annealing, reflecting phase separation in the Fe-Cr system. Inhomogeneity was not considered in the calculation but could be the origin of the smaller negative spin polarization observed in the experiment.

3. Inelastic X-ray scattering

An inelastic X-ray scattering (IXS) spectrometer for hard X-rays installed in EH2 is used for resonant inelastic X-ray scattering (RIXS) at the K-edge of the 3*d* transition metals and the L-edge of the 5*d* transition metals. The optics of EH2 provides an energy resolution of 0.1–1 eV for both incident and scattered (emitted) X-rays. High-energy-resolution fluorescence-detected X-ray absorption spectroscopy (HERFD-XAS) and X-ray emission spectroscopy (XES) are also available using the spectrometer.

In the IXS spectrometer working thus far, both scattering planes of the sample (through source, sample, and analyzer) and analyzer (through sample, analyzer, and detector) are horizontal. While measurements under the grazing-incidence condition enhance the scattering intensity from thin samples, the scattering plane of the analyzer parallel to that of the sample prevents us from applying the grazing-incidence condition. This is because a horizontally elongated beam spot on the sample degrades the energy resolution. This restriction is

lifted if the scattering planes of the sample and analyzer are orthogonal. To realize a vertical scattering plane of the analyzer, we mounted two translation stages and one rotation stage on the spectrometer. These stages mimic a 2θ-arm for the scattering from the analyzers. We also installed a device to rotate the analyzer stage by 90°. The system with the vertical scattering plane shown in Fig. 2 enables us to measure thin samples efficiently using the grazing-incidence condition.

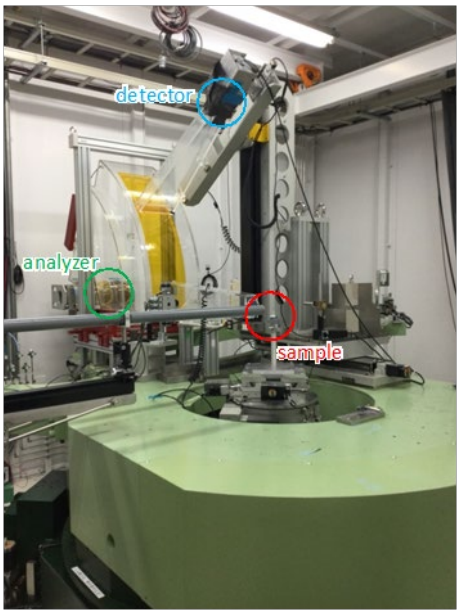

Fig. 2. IXS spectrometer with the vertical scattering plane of the analyzer.

4. X-ray magnetic circularly polarized emission

X-ray magnetic circularly polarized emission (XMCPE) is a phenomenon in which characteristic X-rays emitted from a magnetized material are circularly polarized [2]. An advantage of XMCPE is the large flipping ratio (~25%) in the hard X-ray region for 3*d* transition metal elements. This feature is well suited for observations of magnetic microstructures well below the sample surface.

The development of a bulk-sensitive magnetic microscope utilizing XMCPE started in FY2018 at BL11XU, and a scanning X-ray magnetic microscope with a lateral resolution of 10 μm was successfully constructed in FY2020 [3]. With this microscope, magnetic domains in grain-oriented electrical steel have been investigated.

5. Surface X-ray diffraction

The third experimental hutch is equipped with a surface X-ray diffractometer connected with a molecular beam epitaxy (MBE) chamber [4,5]. This instrument is designed for *in situ* studies on III–V group semiconductor surfaces, especially surface crystallography under MBE conditions and growth dynamics of multilayer and nanostructures. The III–V group semiconductors are nitrides such as GaN and InN and arsenides such as GaAs and InAs, which can be grown by exchanging the two types of MBE chamber.

Our recent activity on the nitrides focuses on the growth of (In)GaN films that are applicable for optoelectronic devices [6,7]. *In situ* X-ray diffraction reciprocal space mapping (*in situ* RSM) measurement using our surface X-ray diffractometer is a powerful tool for characterizing (In)GaN film properties such as lattice strain and indium composition from the results of the evolution of (In)GaN diffraction peaks. We carried out the radio-frequency (RF) plasma-assisted MBE growth of InGaN on GaN and InN layers, which were also grown by RF-MBE on commercialized GaN/*c*-sapphire templates. Different initial growth behaviors of InGaN, especially the incorporation of indium atoms, could be observed depending on the underlying material properties.

Another substrate material of (In)GaN film growth is a graphene-covered SiO_2 or graphene

grown on c-sapphire substrates. Because the graphene weakly interacts with the substrates, (In)GaN growth on the graphene allows us to produce freestanding high-quality (In)GaN films even though there is a high lattice mismatch between (In)GaN and the substrate materials. Using *in situ* RSM, we observed the evolution of lattice strain and indium composition of the (In)GaN films grown on the graphene substrates and determined the optimum growth conditions. On the basis of our experimental results, (In)GaN growth on graphene substrates could lead to the fabrication of freestanding (In)GaN films by mechanical exfoliation, which would be useful for flexible devices.

Mitsui Takaya[*1], Inami Toshiya[*1], Ishii Kenji[*2], and Sasaki Takuo[*3]

[*1]Magnetism Research Group, National Institutes for Quantum Science and Technology (QST)

[*2]Advanced Spectroscopy Research Group, National Institutes for Quantum Science and Technology (QST)

[*3]Coherent X-ray Research Group, National Institutes for Quantum Science and Technology (QST)

References:

[1] Suto, H. Nakatani, T. Kota, Y. Asam, N. Iwasaki, H. Amemiya, K. Mitsui, T. Sakai, S. Li, S. & Sakuraba, Y. (2022). *J. Magn. Magn. Mater.* **557,** 16974.

[2] Inami, T. (2017). *Phys. Rev. Lett.* **119**, 137203.

[3] Sugawara, K. Inami, T. Nakada, T. Sakaguchi, Y. & Takahashi, S. (2021). *J. Appl. Phys.* **130**, 113901.

[4] Takahasi, M. (2013). *J. Phys. Soc. Jpn.* **82**, 021011.

[5] Sasaki, T. et al. (2016). *Jpn. J. Appl. Phys.* **55**, 05FB05.

[6] Yamaguchi, T. et al. (2019). *Crystals* **9**, 631.

[7] Fuke, S. et al. (2020). *Jpn. J. Appl. Phys.* **59**, 070902.